Coral Reefs
DOI 10.1007/s00338-014-1162-1

REPORT

Forecasting decadal changes in sea surface temperatures and coral bleaching within a Caribbean coral reef

Angang Li · Matthew A. Reidenbach

Received: 10 August 2013 / Accepted: 29 April 2014

Abstract Elevated sea surface temperature (SST) caused by global warming is one of the major threats to coral reefs. While increased SST has been shown to negatively affect the health of coral reefs by increasing rates of coral bleaching, how changes to atmospheric heating impact SST distributions, modified by local flow environments, has been less understood. This study aimed to simulate future water flow patterns and water surface heating in response to increased air temperature within a coral reef system in Bocas del Toro, Panama, located within the Caribbean Sea. Water flow and SST were modeled using the Delft3D-FLOW© computer simulation package. Locally measured physical parameters, including bathymetry, astronomic tidal forcing, and coral habitat distribution were input into the model and water flow, and SST was simulated over a four-month period under present day, as well as projected warming scenarios in 2020s, 2050s, and 2080s. Changes in SST, and hence the thermal stress to corals, were quantified by degree heating weeks. Results showed that present-day reported bleaching sites were consistent with localized regions of continuous high SST. Regions with highest SST were located within shallow coastal sites adjacent to the mainland or within the interior of the bay, and characterized by low currents with high water retention times. Under projected increases in SSTs, shallow reef areas in low flow regions were found to be hot spots for future bleaching.

Communicated by Biology Editor Prof. Brian Helmuth

A. Li · M. A. Reidenbach (✉)
Department of Environmental Sciences, University of Virginia, Charlottesville, VA 22904, USA
e-mail: reidenbach@virginia.edu

Keywords Climate change · Coral reefs · Sea surface temperature · Coral bleaching

Introduction

A primary direct consequence of global warming is increasing sea surface temperature (SST; Bindoff et al. 2007). From the 1950s to 2009, the mean global SST has increased by approximately 0.4 °C (Levitus et al. 2009), which has had profound and diverse impacts on marine ecosystems (Doney et al. 2012), including coral reefs. Coral reefs provide crucial ecosystem services, including shoreline protection (Wilkinson 1996; Bradley et al. 2009), tourism benefits (Reaser et al. 2000; Rehr 2012), and shelter for one-quarter of all known marine species (Pratchett et al. 2009; Thur 2010). Projected increases in SST may cause coral reefs to disappear entirely within 20–50 yrs if corals cannot adjust to tolerate this increased heating (Hoegh-Guldberg et al. 2007). Consequently, it is important to determine how atmospheric and ocean heating affects the spatial distribution of SST surrounding reef areas. Such patterns in SST highlight potential perturbations to coral reef ecosystems, reveal possible shifts in species richness and abundance, and suggest vulnerable areas that might be prioritized for marine conservation efforts.

Studies have shown that SST anomalies are the major cause of mass coral mortality, which is initiated through coral bleaching (Hughes et al. 2003; Donner 2009). When SST exceeds the historical mean of local summer maxima by 1–2 °C for 3–4 weeks (Hoegh-Guldberg 1999), coral bleaching occurs due to the loss of endosymbiotic dinoflagellates (*Symbiodinium* spp.) or their photosynthetic pigments (Glynn 1993). These symbiotic algae fuel 95 % of the metabolic activity of their coral hosts (Hoegh-

Published online: 10 May 2014

Guldberg et al. 2007; Donner 2009). Even though the actual temperature threshold of coral bleaching depends on reef location and coral species (Hughes et al. 2003), thresholds at most locations range from 29 to 32 °C (Baird et al. 2009), and SST anomalies of <1 °C may exceed physiological tolerances (Walther et al. 2002) and cause large-scale bleaching. While coral bleaching does not necessarily result in coral death, thermal stress typically leads to reduced growth rate and fecundity, and partial bleaching tends to make corals more vulnerable to disease (Harvell et al. 2002; Bruno et al. 2007; Muller et al. 2008).

Studies have observed that the spatial distribution of SST and occurrence of coral bleaching are patchy, both within a reef and among reefs (Berkelmans and Oliver 1999; Jokiel and Brown 2004; Ateweberhan and McClanahan 2010). Such variations originate from different environmental factors in each local region (Glynn 1993). Solar radiation, in the form of photosynthetically active radiation (PAR, 400–700 nm) and ultraviolet radiation (UVR, 290–400 nm; Lesser and Farrell 2004), can inhibit photosynthesis within corals by causing photosynthetic organisms to produce an excess flux of toxic reactive oxygen species (Lesser et al. 1990; Lesser 1996), or by damaging photosystems and reducing carbon fixation in corals exposed to elevated temperature (Lesser 1996; Ferrier-Pages et al. 2007). Restricted water circulation within bays and lagoons can result in retention of water and localized heating above offshore values (Jokiel and Brown 2004). Within coral reefs of the Red Sea, Davis et al. (2011) found that the greatest diurnal variation in water temperatures occurred near the center of larger reef flats and on reefs that are protected from direct wave forcing, while less diurnal temperature variability occurred on smaller knolls or along the edge of reef flats. Doldrums, periods of exceptionally warm water coupled with calm weather (Hoegh-Guldberg 2011), amplify the warming of the sea surface by reduced vertical mixing due to low wind speed and intense heating (Berkelmans et al. 2010). Strong ocean winds, on the contrary, reduce SST through enhanced evaporative cooling and by mixing warm surface water with cool deeper water (Manzello et al. 2007). Within shallow reef areas, solar radiation penetrating to the benthos may also be strong enough to heat the seafloor and affect the thermal environment of benthic organisms (Wells et al. 2012).

While observations and mechanisms of these environmental impacts on coral reefs have attracted much attention, the prediction of how local SST responds to local environmental factors, and thus exerts different impacts on corals, has seen less focus. Historically, synoptic forecasts of elevated SST have been used almost exclusively to predict coral bleaching (Aronson et al. 2002; Liu et al. 2006). Specifically, a suite of satellite products, developed by NOAA Coral Reef Watch, has been forecasting global SST (Peñaflor et al. 2009) at a resolution of approximately 50 km with a lead time of 3 months and has effectively predicted severe bleaching events (Reynolds and Smith 1994; Reynolds et al. 2005). However, these SST predictions can fall short in real practice, not only due to their relatively short period forecasted, but also due to considerable variations in local SST distribution across spatial scales of <50 km.

The main objectives of this study were (1) to examine the local water flow patterns and SST under present-day scenarios utilizing both in situ observations and a numerical model (Delft3D-FLOW©), (2) to simulate heating scenarios in the 2020s, 2050s, and 2080s under predicted global warming, and (3) to quantify local thermal stress on coral reefs in comparison with existing coral bleaching records. We hypothesize that, under projected atmospheric warming, more shallow regions than offshore areas will reach SST that exceed coral maximum threshold temperatures, and it is those shallow regions that have a tendency to induce intensive coral bleaching. Our study site is the coral reef ecosystem fringing the Bocas del Toro archipelago, Panama, located in the southwest Caribbean Sea. This site was chosen due to the existing long-term climate and oceanographic records as well as coral bleaching information within the region (Guzmán et al. 2005).

Materials and methods

Study site

The study site (Fig. 1) is the coral reef ecosystem along the Bocas del Toro archipelago. The Bocas del Toro archipelago forms a shallow bay that is almost entirely surrounded by land, and, due to the restricted nature of water circulation, inshore waters have significantly higher means and ranges of SST compared to offshore waters (Kauffman and Thomson 2005). As such, the vast coral reefs, which inhabit the shallow water surrounding the archipelago islands and along the mainland coast down to 25 m deep, may experience substantially different water temperatures from inshore to offshore. Correspondingly, observations of coral bleaching (Fig. 1) have been reported in the year 2002 and 2005 at water depths ranging from 0.5 to 9.6 m (ReefBase 2013), with low to medium severity in general within the study site.

Oceanographic and meteorological data were collected at 15-min intervals from a weather station (9°21′02.96″N; 82°15′28.27″W) located approximately 100 m offshore of the Smithsonian Tropical Research Institute (STRI) station in Bocas del Toro, Panama. The physical variables measured at the station include incident solar radiation (Q_s), air temperature (T_a), seawater temperature (T_w), relative air humidity (r_{hum}), cloud fraction (F_c), wind speed at 10 m

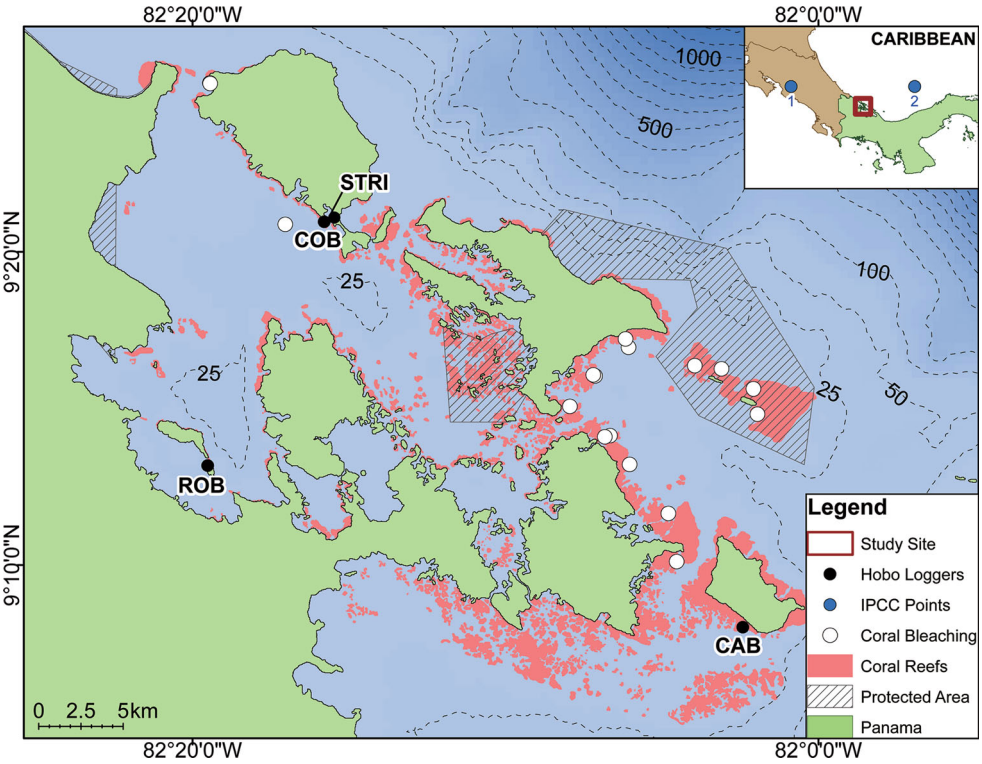

Fig. 1 Site map of the Bocas del Toro archipelago, with the location of the study area marked by a hollowed *red square* within the *inset* image. Within main image, positions of hobo loggers are represented by *black circles*, *points* of the IPCC prediction sites (2003) by *blue circles*, observational spots of coral bleaching (ReefBase 2013) by *white circles*, distribution of coral reefs (UNEP-WCMC 2010) by *red patches*, marine protected area (IUCN and UNEP-WCMC 2010) by *polygon shadows*, and the Panama base map (ESRI 2010) by *green patches*. Bathymetry contours are of 100-m increments starting from 100 m depth

above the sea surface (U_{10}), wind direction, and water level (ζ). These datasets were chosen to represent the local environment of the study site, while additional temperature sensors (HOBO data-loggers, Fig. 1) were deployed from 2006 to 2010 by STRI staff to measure hourly water temperatures at various locations throughout the region. These temperature loggers provide 12-bit resolution and ±0.2 °C accuracy. Temperature loggers were located in Isla Colón (COB) at a depth of 4.6 m, Isla Cayo Agua (CAB) at 5.2 m, and Isla Roldan (ROB) at 4.6 m (Table 1). In addition, a vertical temperature profile was also recorded every 15 min at COB at 4.6, 9.1, and 18.3 m from July to October 2010. Differences in water temperatures between the depths were consistently <0.2 °C, which was within the ±0.2 °C accuracy of the temperature loggers, suggesting vertically well-mixed conditions across this depth range. Previous studies have shown that spatial differences in SST are not appreciably affected by rainfall and freshwater runoff, but instead are primarily determined by shoreline geometry, solar radiation, and wind speed (Guzmán et al. 2005; Kauffman and Thomson 2005). Therefore, the effects of river runoff and rainfall on SST were not addressed in this study.

To validate the numerical flow model, a Nortek Inc. Aquadopp© high-resolution velocity profiler was deployed during August 2011 during a 5-d period to obtain velocity profiles throughout the water column. The Aquadopp measured 3-D velocities within bins spaced at a 0.03 m vertical elevation within the water column, at a sampling rate of 1 Hz. The Aquadopp was secured on a frame and deployed on the seafloor at a mean water depth of 1.5 m, at a site approximately 1 km offshore from the STRI station (9°21′7.62″N; 82°15′55.92″W). A Richard Branker Research TWR-2050P submersible tide and wave recorder was also deployed adjacent to the Aquadopp to measure wave statistics. The TWR-2050P sampled water pressure at 4 Hz for 3-min bursts every h.

Table 1 List of the four environmental datasets used in this study

Code	Location	Variables measured	Depth of T_w measured (m)	Time interval (min)
STRI	STRI station	T_w, Q_s, etc.	2.0	15
COB	Isla Colón	T_w	4.6	60
CAB	Isla Cayo Agua	T_w	5.2	60
ROB	Isla Roldan	T_w	4.6	60

Water temperature (T_w) data were measured at different locations and depths within the Bocas del Toro Archipelago

Heating scenarios

The time frame July–October of 2010 was selected as the 'present-day' setting for this study. In addition, the hourly water temperature data collected at the four sites from 2006 to 2010 were used to determine the intraannual pattern of water temperatures across the study area (Fig. 2). The

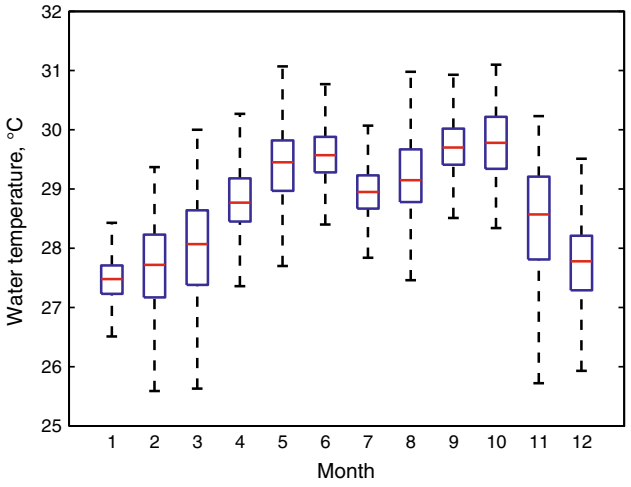

Fig. 2 Intraannual variability of water temperature from 2006 to 2010, based on hourly water temperature data collected from the four HOBO sites (Fig. 1). The *box diagrams* show the medians (*horizontal lines*), the 25th and 75th ‰ (*lower* and *upper rectangle edges*), and *whiskers* extending to the furthest points within each month

month with the lowest monthly median water temperature was January (27.5 °C), and the month with the highest median water temperature was October (29.8 °C), followed by September (29.7 °C), June (29.6 °C), May (29.4 °C), and August (29.2 °C). Hence, August–October was selected to represent the continuous three-month period in which the study site was the most heated. Additionally, July was added to the time frame as the spin-up time allowing the numerical model to stabilize.

The datasets from the STRI station were used to represent the local weather across the study domain from July to October 2010, while the monthly mean weather patterns predicted by the Intergovernmental Panel on Climate Change (IPCC 2003) were applied for July–October in 2024, 2054, and 2084 (Table 2). Two IPCC prediction points most adjacent to the study site were selected (Fig. 1) and spatially interpolated to determine the parameters Q_s, T_a, T_w, r_{hum}, F_c, and U_{10} within each of the future time periods studied. These parameters were used within the numerical model to determine heat flux estimates at the water surface. Site 1 and Site 2 were weighted 1/3 and 2/3, respectively, to allow for a greater Caribbean Sea influence on these variables. To calibrate IPCC predictions, the monthly mean weather data for July–October 2010 were generated (e.g., Table 2a–July) and were compared with the monthly means from the STRI site observations. To adjust for localized changes in the variables, Q_s, T_a, r_{hum}, and U_{10} across the study domain, the ratios of observed means from the STRI site observations to predicted means from IPCC in each month of 2010 were computed. This ratio was then used to adjust the mean IPCC predictions in 2024, 2054, and 2084 (e.g., Table 2b–July). Time series of Q_s, T_a, T_w, r_{hum}, and U_{10} were then generated

Table 2 IPCC predictions of July weather data (a) after spatial interpolation across the study site within each scenario: 1961–1990, 2010–2039 (2020s), 2040–2069 (2050s), and 2070–2099 (2080); (b) followed by temporal interpolation for year 2010 and calibration with the STRI site datasets

July of year	Q_s (W m^{-2})	T_a (°C)	T_w (°C)	r_{hum} (%)	F_c (%)	U_{10} (m s^{-1})
(a)						
1961–1990	194.1	26.1	26.8	85.0	74.7	1.8
2010–2039	194.9	27.0	27.7	84.7	71.5	1.9
2040–2069	204.7	28.2	28.7	81.7	64.2	2.2
2070–2099	218.0	29.8	30.3	76.8	57.7	2.3
(b)						
2010	168.5	27.0	27.3	87.2	65.6	1.6
2024	168.8	27.3	27.7	87.1	64.0	1.6
2054	177.3	28.5	28.7	83.9	56.6	1.9
2084	188.8	30.1	30.3	78.9	52.1	2.0

at 15-min intervals for future scenarios and applied at each time step in the hydrodynamic model.

Model setup

The hydrodynamic model implemented to simulate local water flow and SST was the open-source Delft3D-FLOW, which solves the nonlinear shallow water equations derived from the three-dimensional Navier–Stokes equations for incompressible free surface flow (Lesser et al. 2004; Kernkamp et al. 2005). This model was run in a two-dimensional (2D) mode, and vertically homogeneous conditions were assumed (Kauffman and Thomson 2005). Therefore, computed water flow and SST estimates are depth-averaged values. The same domain of the 2D model was used for all four simulations consisting of July–October in 2010, 2024, 2054, and 2084.

The computational grid (Fig. 3), encompassing all the adjacent bays in addition to the study site, extended offshore to a distance of at least 20 km from the study site to minimize errors occurring at the open boundary. The model domain was partitioned using a Cartesian, curvilinear, orthogonal grid cell arrangement that contained 514 × 246 nodes to cover approximately 7,000 km^2 of water surface area. The model grid had space-varying resolution that allowed for a grid resolution of ≤250 m within the study site, to a coarser horizontal resolution of approximately 400 m on the offshore boundary. The available bathymetry data (Table 3), however, had coarser resolution (926 m) than the grid resolution, such that multiple small islands were not recognized. To better represent the shoreline changes, the bathymetry assigned for each grid cell was determined by a combination of available topography datasets. The shoreline data were implemented to define the actual contour of 0 m in bathymetry. Bounded by

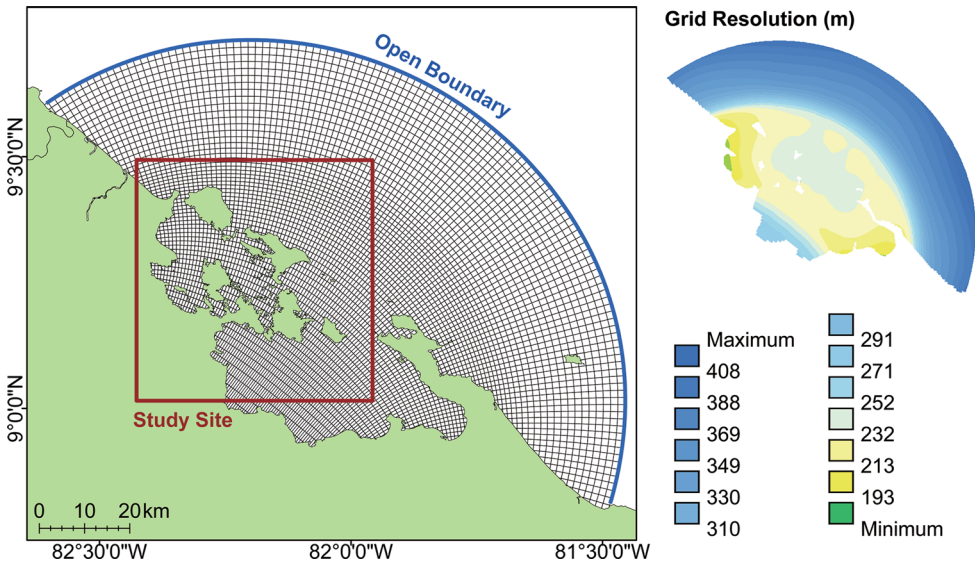

Fig. 3 Computational grid (*left*) and grid resolution (*right*) over the study site at Bocas del Toro. Note that because of the high spatial resolution of the grid, for visualization purpose, the edges of only every 4 × 4 actual cells are shown on the *left*. The *continuous shade on the right* indicates the space-varying resolution of the actual grid

Table 3 List of available topography datasets provided by Delft DashBoard (DDB) over the Bocas del Toro archipelago

Database	Coverage	Resolution (m)	Year updated
GEBCO	Ocean	926	2008
SRTM	Land	93	2008
WVS	Shoreline	<500	2013

The databases were originally collected by DDB from various sources: GEBCO bathymetry data from the British Oceanographic Data Centre (BODC), SRTM land elevation data from Jarvis et al. (2008), and the WVS shoreline data from the National Geospatial-Intelligence Agency (NGA)

the shoreline, the land elevation data were projected onto the model grids using triangular interpolation to identify small islands at a resolution of 93 m. Similarly bounded, the projected General Bathymetric Chart of the Oceans (GEBCO) bathymetry was added to the empty grids. The remaining grid cells were filled by internal diffusion followed by further smoothing along selected shoreline segments.

Based on the grid and bathymetry of the domain, the time step of the simulation to ensure numerical stability and accuracy of the model, as indicated by the Courant number (C) for 2D models (Stelling 1984), was determined as:

$$C = 2\Delta t\sqrt{gh\left(\frac{1}{\Delta x^2}+\frac{1}{\Delta y^2}\right)} \quad (1)$$

where Δt is the time step (s), g is the acceleration of gravity (m s^{-2}), h is the local water depth (m), and Δx and Δy are grid lengths in x and y directions (m) within each cell. For locations with large differences in bottom geometry or coastline, the C should not exceed a value of ten. Constrained by this characteristic Courant value, a time step of $\Delta t = 6$ s was adopted in the simulation to maintain the accuracy and stability over the entire domain.

Flow boundary conditions

Starting from an initial condition of a uniform water level of $\zeta = 0$ m over the entire domain, the flow was primarily forced by tides at the open boundaries and wind stress at the free surface, while drag was imposed at the sea bed by bottom roughness. Along the offshore open boundary (Fig. 3), water level conditions induced by astronomical tides were defined using thirteen tidal constituents (M2, S2, N2, K2, K1, O1, P1, Q1, Mf, Mm, M4, MS4, and MN4) extracted from the database TPXO 7.2 Global Inverse Tide Model (Egbert et al. 1994; Egbert and Erofeeva 2002). At the free surface, the effect of wind stress was applied via spatially uniform wind speed and wind direction data at 15-min intervals for each scenario. While the wind speed data varied from year to year based on IPCC predictions, the wind direction time series in July–October were assumed to be the same throughout the simulated years. At the seafloor, a spatially varying bottom roughness was developed using Manning's n roughness coefficients of 0.02 for hardground, 0.035 for sea grass, and 0.05 for coral reef locations (Prager 1991; Madsen et al. 2001; Reidenbach et al. 2006). Spatial distribution of these benthic habitats, namely coral reefs (IMaRS-USF and IRD 2005; IMaRS-USF 2005) and sea grasses (Green and Short 2003), was retrieved from United Nations Environmental Program-World Conservation Monitoring Center (UNEP-WCMC and Short 2005; UNEP-WCMC 2010).

Heat flux

An initial heat condition was uniformly applied over the domain using monthly mean T_w values of July for each scenario (Table 2b). Heat flux at the water surface was

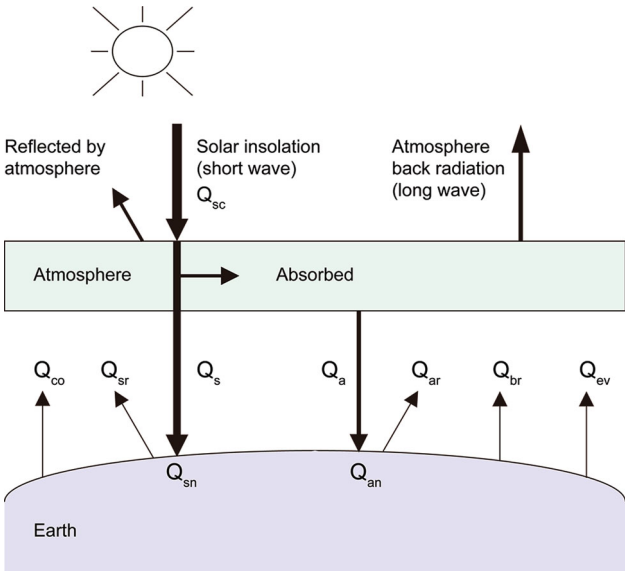

Fig. 4 Heat exchange mechanism at the earth's water surface, where Q_{sc} is the solar insolation (J m^{-2} s^{-1}), Q_s is the solar radiation (J m^{-2} s^{-1}), Q_{sr} is the reflected solar radiation (J m^{-2} s^{-1}), Q_a is the atmospheric radiation (J m^{-2} s^{-1}), Q_{ar} is the reflected atmospheric radiation (J m^{-2} s^{-1}), Q_{br} is the back radiation (J m^{-2} s^{-1}), Q_{ev} is the latent heat flux (J m^{-2} s^{-1}), and Q_{co} is the sensible heat flux (J m^{-2} s^{-1}). The combination of net solar radiation ($Q_{sn} = Q_s - Q_{sr}$) and net atmospheric radiation ($Q_{an} = Q_a - Q_{ar}$) serves as the energy input to the surface

simulated within the Delft3D-FLOW model and driven by meteorological variables (Fig. 4), and governed by the heat balance equation (Gill 1982):

$$Q_{tot} = Q_{sn} + Q_{an} - Q_{br} - Q_{ev} - Q_{co} \quad (2)$$

where Q_{tot} is the total heat flux (W m^{-2}), Q_{sn} is the net solar radiation (W m^{-2}), Q_{an} is the net atmospheric radiation (W m^{-2}), Q_{br} is the back radiation (W m^{-2}), Q_{ev} is the latent heat flux (W m^{-2}), and Q_{co} is the sensible heat flux (W m^{-2}). T_w was then simulated by quantifying vertical energy exchange at the air–water interface and horizontal advective heat transfer due to fluid motion (Webb and Zhang 1999; Hannah et al. 2004, 2008). The model was prescribed by spatially uniform variables r_{hum}, T_a, Q_{sn}, and F_c, of which Q_{sn} was derived from:

$$Q_{sn} = (1 - \alpha)Q_s \quad (3)$$

where $\alpha = 0.06$ is the albedo coefficient defined within the model. F_c was calculated through the function (Gill 1982):

$$1.0 - 0.4F_c - 0.38F_c^2 = \frac{Q_s}{Q_{sc}} \quad (4)$$

Q_{sc} (W m^{-2}) is the incident solar radiation for clear sky conditions (Gill 1982),

$$Q_{sc} = \begin{cases} 0.76S\sin(\gamma) & \sin(\gamma) \geq 0 \\ 0.0, & \sin(\gamma) < 0 \end{cases} \quad (5)$$

where $S = 1{,}368$ W m^{-2} is the solar constant, and γ (°) is the solar elevation angle (Grena 2012).

Model validation and sensitivity analysis

To quantify the ability of the model to predict SST within the study site, preliminary simulations were conducted for a period between 1 July and 10 August 2010. Simulated water temperatures at the end of the time period were compared with the observed values at the four temperature logger sites (Fig. 1) using a goodness-of-fit (GoF) function over time (t), layer ($\sigma = 1$), and model domain (n, m):

$$\mathrm{GoF} = \frac{\left\{\sum_t \sum_\sigma \sum_{n,m} \left\{W_{t,\sigma,n,m} \times \left|y_{t,\sigma,n,m} - x_{t,\sigma,n,m}\right|\right\}\right\}}{\left\{\sum_t \sum_\sigma \sum_{n,m} \left\{W_{t,\sigma,n,m}\right\}\right\}} \quad (6)$$

where $W = 1/4$ denotes the weight function, y represents the model-simulated SST, and x the observed SST. The sets of coefficients tested were (1) the Stanton number (c_H) that controls the magnitude of the convective heat flux and the Dalton number (c_e) for the evaporative heat flux, (2) the horizontal eddy diffusivity (D_H) and horizontal eddy viscosity (ν_H), which were set equal to each other (Boudreau and Jorgensen 2001) and specify the magnitude of turbulent mixing, and (3) the wind drag coefficient (C_d) that prescribes the magnitude of the surface wind stress. The resulting GoF, allowing for spatial and temporal variations in model performance, reflects increasing model quality with decreasing values.

We investigated the influences of the three-parameter sets by varying each parameter independently over a wide range of physically reasonable values. Values of c_H ranged from 7.9×10^{-3} to 2.255×10^{-3}, while c_e ranged from 1.2×10^{-3} to 1.885×10^{-3} (Gill 1982). c_H and c_e were both tested using a step size of 0.5×10^{-3} from 1×10^{-3} to 2×10^{-3}. The magnitudes of D_H and ν_H were tested for values between 10^{-1} and 10^2 m^2 s^{-1} within the possible range for coastal settings. In addition, while the magnitude of C_d showed a strong regional dependency, most of the values fall within the range of 0.5×10^{-3}–1.5×10^{-3} as indicated by empirical formulas (Garratt 1977; Heaps 1965) and therefore were assessed between this range at 0.5×10^{-3} intervals, in addition to the baseline value 0.63×10^{-3}. The resulting minimum values of the GoF were found at $c_H = 2 \times 10^{-3}$, $c_e = 1 \times 10^{-3}$, $D_H = \nu_H = 10$ m^2 s^{-1}, and $C_d = 0.5 \times 10^{-3}$. Due to the minimal change of the GoF values across the range of C_d, the value $C_d = 0.63 \times 10^{-3}$ was chosen, consistent with the original heat flux formulation. Overall, the GoF value was reduced from 0.385 °C in the initial setup to 0.236 °C in the optimized run, showing a 39 % decrease in the

Table 4 Comparison of the setup of model runs and their GoF values with respect to the water temperature data observed at the four temperature logger sites (Fig. 1) in August 01–August 10, 2010

Setup	c_H	c_e	$D_H = \nu_H$ (m^2 s^{-1})	C_d	GoF (°C)
Initial	0.00145	0.0015	1	0.00063	0.385
Optimized	0.002	0.001	10	0.00063	0.236

disagreements between the model results and observations (Table 4).

In addition to the overall model performance evaluated by GoF, a normalized skill score termed the index of agreement (IAS) was applied to compare model predictions to in situ observations in the 2010 scenario at each individual observation site. The IAS is defined as (Willmott 1982; Warner et al. 2005):

$$\mathrm{IAS} = 1 - \frac{\sum (y - x)^2}{\sum \left(|y - \bar{x}| + |x - \bar{x}|\right)^2} \quad (7)$$

where the over-bar denotes a time average. An *IAS* value of 1.0 corresponds to a 100 % agreement between model prediction of SST, y, and observations of SST, x, while decreasing values indicate decreasing agreement, or poorer model performance.

Degree heating weeks

The cumulative thermal stress to the coral reef ecosystem was quantified based upon 'degree heating weeks' (DHW), in the same way as NOAA Coral Reef Watch program uses DHW from satellite-derived SST. Specifically, DHW (°C week) is calculated by summing the positive deviations (whenever ≥1 °C) of the weekly average SST over a 12-week period (Eakin et al. 2009; Strong et al. 2006):

$$\mathrm{DHW} = \sum (\mathrm{SST} - \mathrm{MMM}) \quad (8)$$

where MMM is the maximum monthly mean (°C) calculated by choosing the mean temperature during the warmest month of the year. In this study, the MMM value of 28.5 °C was used based on data from the NOAA 50 km local monthly mean satellite-only nighttime SST. The same alert levels as NOAA (summarized in Table 5) were used, where a 'Warning' is issued when DHW >0 °C weeks, a coral bleaching 'Alert Level 1' when values near a reef reach DHW ≥4 °C weeks, and an 'Alert Level 2' when reefs experience DHW ≥8 °C weeks. Mass bleaching and the onset of coral mortality are expected after Alert Level 2.

Table 5 A summary of the alert levels for coral bleaching modified from NOAA (2009)

Status	Interpretation	Definition
Warning	Thermal stress is accumulating	DHW >0
Alert Level 1	Bleaching expected	DHW >4
Alert Level 2	Widespread bleaching and some mortality expected	DHW >8

The alert levels are based on DHW for each site

Results

Model validation

Based on the optimized model setup, the predicted variations in water level ζ (Fig. 5) and water temperature T_w (Fig. 6) show good consistency with the observed patterns within the model domain between August and October 2010. The best tidal agreement between model and observations occurred at the STRI site with an IAS of 0.937. The T_w prediction at STRI, however, reproduced less of the high-frequency temperature fluctuations observed in situ, but the overall trend was in agreement. While COB and CAB saw slightly better model agreement in predicting T_w than STRI, site ROB had greater deviations, and overall lower modeled water temperatures compared to observations due to its location within the inner lagoon area, far away from the open boundary tidal forcing. The IAS values were shown to be relatively high in general, ranging from 0.593 to 0.937 (Table 6). The depth-averaged water velocity (mean ± SD) obtained in situ at a site approximately 1 km offshore from the STRI site was 1.36 ± 0.69 cm s^{-1}, which compared well to model results at the same location of 1.47 ± 1.02 cm s^{-1}. The average significant wave height during this period was 2.8 ± 2.6 cm, with a maximum wave height of 8.4 cm, suggesting that waves are typically very small within the protected bays.

Flow and SST

Instantaneous flow magnitude and velocity vectors modeled for 20 August 2010 are shown in Fig. 7 and are representative of predominant spatial flow patterns for all four simulated time periods between 2010 and 2084. Maximum water velocities were approximately 0.4 m s^{-1} and were located approximately 2 km offshore. Large reductions in flow magnitude were found along a transect from the offshore to the inshore, such that interior bays of the Bocas del Toro archipeligo had mean flows of approximately 0.05 m s^{-1}. In contrast to these weak flows within interior bays, water flow at several inlets between adjacent islands was quite large, generating periodic flows up to 0.4 m s^{-1}.

Predicted SST for the years 2010 through 2084 is shown in Fig. 8. While the flow patterns showed reduced magnitude from offshore to inshore, an overall reverse gradient of SST occurred, with increasing SST magnitude of approximately 2–3 °C from the offshore to inshore areas.

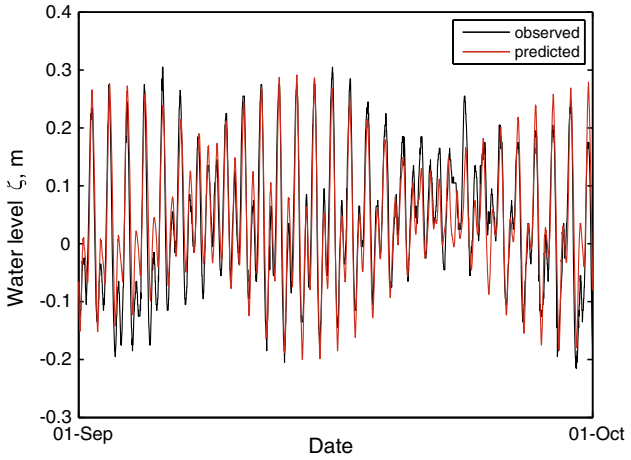

Fig. 5 Comparison of the predicted water level ζ with the observed values at STRI for September 2010

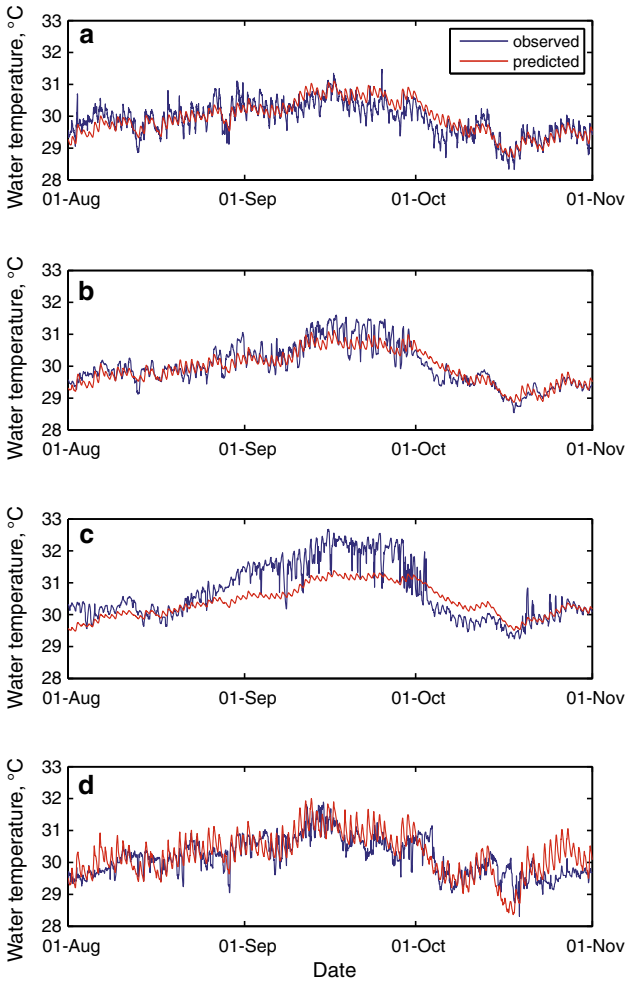

Fig. 6 Comparison of the predicted water temperature T_w with the observed values at the **a** STRI, **b** COB, **c** ROB, and **d** CAB from August to October 2010

Table 6 Index of agreement (IAS), for water level ζ and water temperature T_w between simulations and observations at various locations (Fig. 1) in the model domain

Variable	Location	IAS
ζ	STRI	0.937
T_w	STRI	0.637
T_w	COB	0.711
T_w	ROB	0.593
T_w	CAB	0.773

Values shown are for August–October 2010. Higher IAS values indicate better agreement between the observed and the simulated variables

Temporally, SST increased approximately 1 °C every 30 yr at most locations from 2010 to 2084. By the year 2084, virtually all locations inside or near the interior bays of the Bocas del Toro archipelago reach an SST >31 °C during August.

Degree heating weeks

Derived from the SST predictions, the DHW patterns (Fig. 9) show large variations of the thermally induced stress on coral reef ecosystems at different locations and time periods when compared to the maximum monthly mean of 28.5 °C (Eq. 8). Within each modeled time period, there was an increase in DHW values from the open ocean toward the mainland. The largest magnitudes of DHW were found within the interior bays and adjacent to islands within shallow waters, which often coincided to regions where coral reefs are located. For increasing time periods from 2010, DHW values increased within the bay, from DHW = 0 °C at the open ocean to approximately DHW = 12–16 °C weeks within the bay by the year 2054. In addition to the increase in DHW in regions that had positive DHW under the present-day scenario (2010), the contours of DHW also expanded toward the open ocean in future years, covering an increasingly larger area affected by thermal stress. By the year 2084, all regions within or adjacent to the bay reached DHW >8 °C weeks. In addition, even the open ocean within our study site experienced significantly higher values of DHW.

To determine spatial variations in DHW across the measurement domain, four locations (shown in Fig. 9d) where coral bleaching events had been reported (ReefBase 2013) were chosen. The four bleaching sites started from differing DHW values in 2010, ranging from DHW = 2.3 °C weeks at Site 4 to 9.5 °C weeks at Site 3 (Fig. 10). In spite of large variations in DHW in 2010, the DHW values at the four sites converged to a magnitude of DHW = 18–19 °C weeks in year 2084. While Site 3 had the highest DHW in 2010, its value was exceeded by both

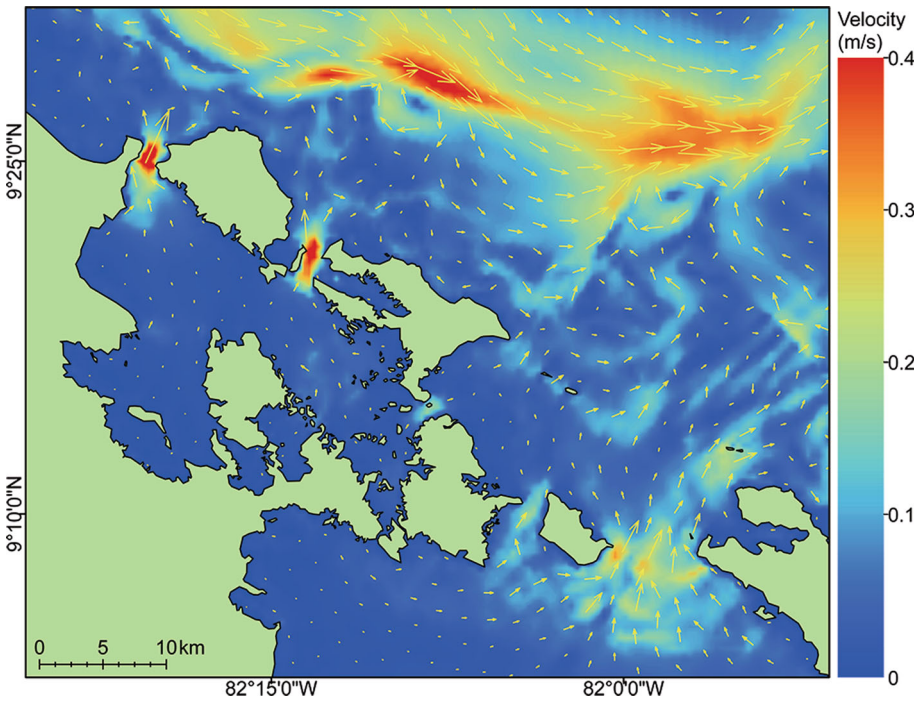

Fig. 7 Predicted magnitude and *vector arrows* of the depth-averaged flow velocities (m s^{-1}) at 0000 hrs on August 20, 2010, as a representative flow pattern within the study site

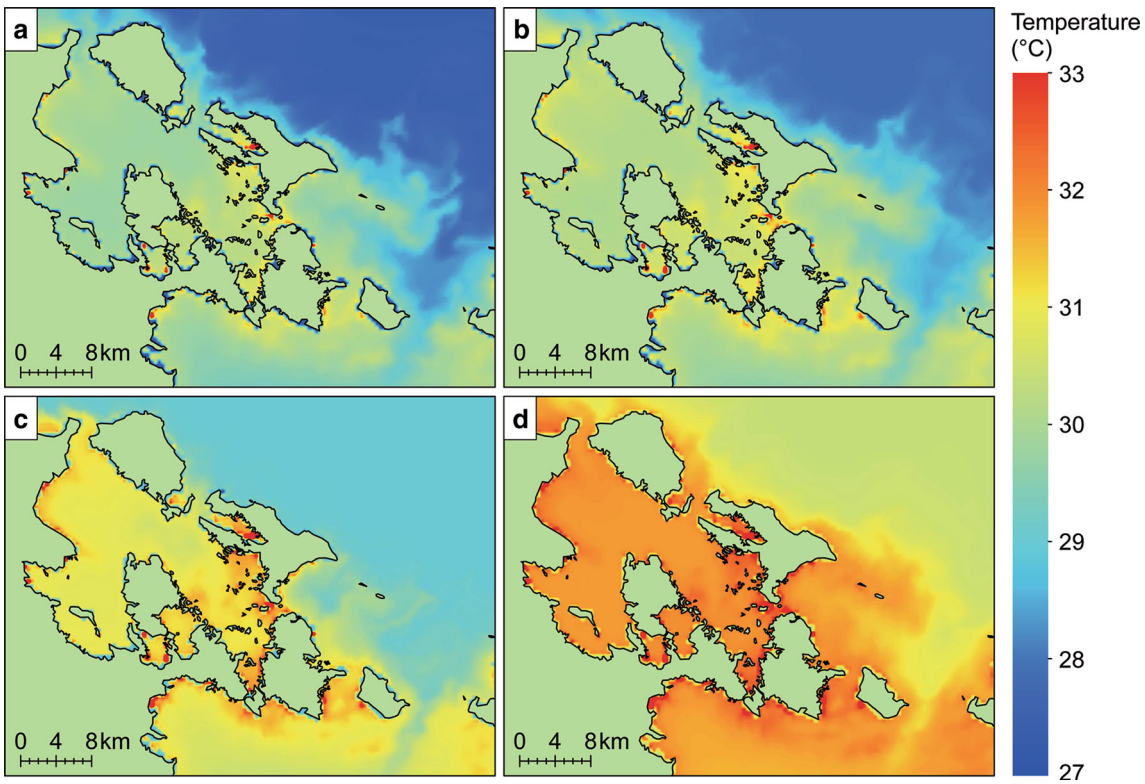

Fig. 8 Predicted SST (°C) distribution at 0000 hrs on 20 August during **a** 2010, **b** 2024, **c** 2054, and **d** 2084. Note higher temperatures along inshore, shallow regions

Site 1 and Site 2 in 2084, by 0.7 and 0.3 °C weeks, respectively. Rapid increases in DHW were especially evident from 2054 to 2084. In particular, Site 4 increased from DHW = 4.8 °C weeks in 2054 to 18.1 °C weeks in 2084. The numerical model predicted that the four sites experienced different thermal stress during different time periods, hence falling into various categories of alert levels (Table 7). Site 3, located inside the bay and close to the

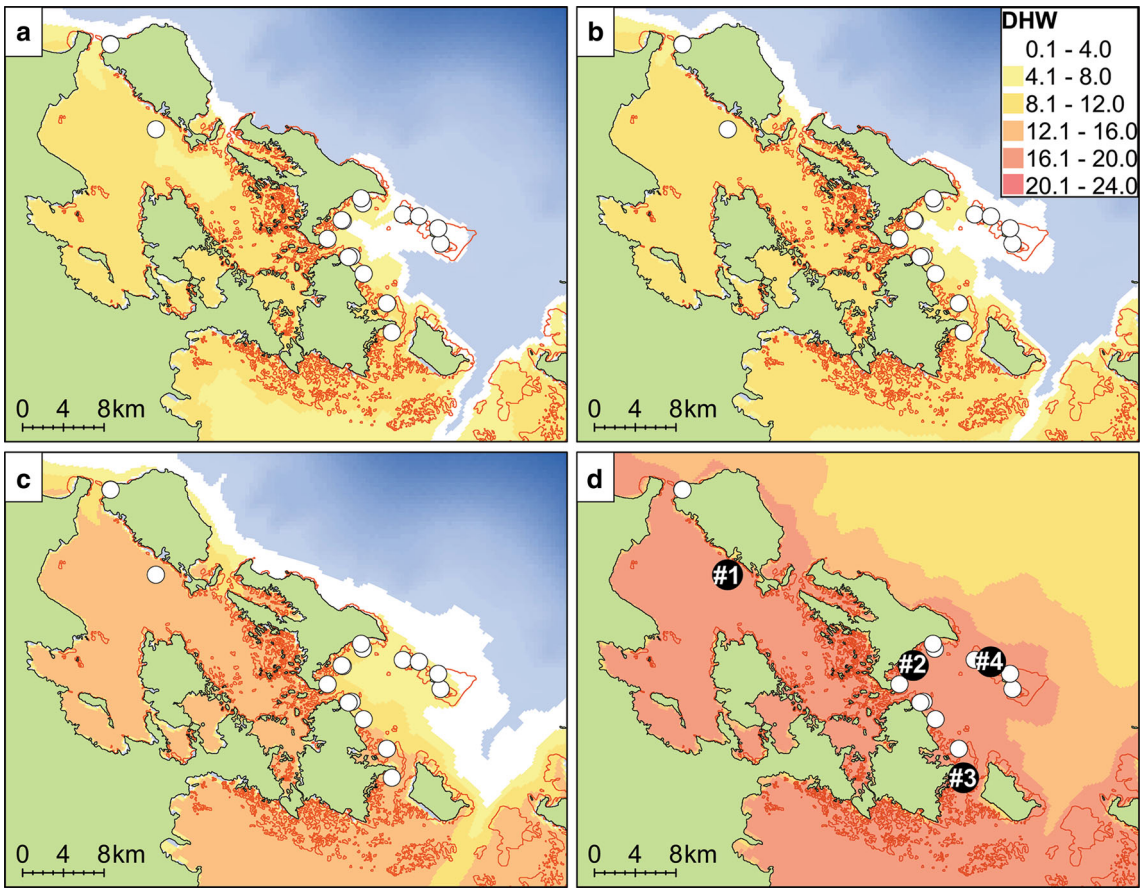

Fig. 9 Degree heating weeks DHW (°C week) within the study site during August–October of **a** 2010, **b** 2024, **c** 2054, and **d** 2084, with *hollowed red polygons* representing coral reefs, *white circles* depicting reported coral bleaching sites, and *black circles* in **d** showing four representative bleaching sites

STRI station, had an Alert Level 2 starting from 2010 and remained at Alert Level 2 for all future years. In contrast to this continuously high level of bleaching alert, the other three bleaching sites, located toward the open ocean, saw lower stress in present day (2010), but had increased alert levels with time. Site 4 had the most drastic change in alert level, from a Warning in 2024 to Alert Level 2 in 2084.

Water retention times

Heating of the water masses, and increased SST, is dependent both upon the water column depth (affecting the surface area to volume ratio of the water) and the magnitude of the exchange flow with the open ocean. To determine the retention time of water masses within specific regions of the model domain, the domain was divided into equivalent 1 km^2 regions, and total water volume (m^3) within each 1 km^2 region, computed as the surface area multiplied by average water depth, was divided by the average volumetric flux of water out of the volume (m^3 s^{-1}) over a spring-neap cycle in August 2010. Here, we define retention time as how long a water parcel, starting from a specified location within

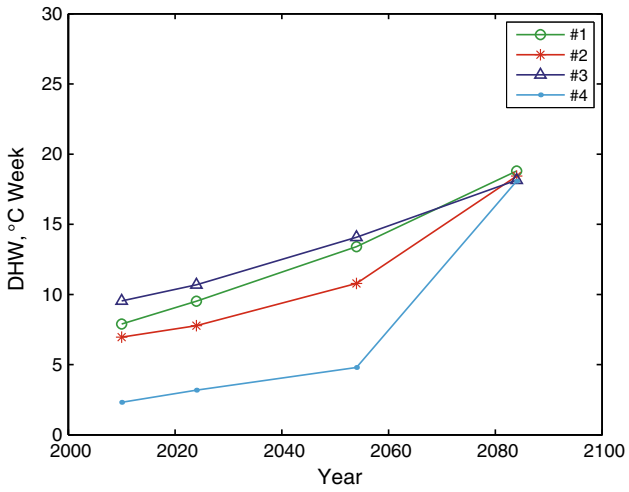

Fig. 10 Trend of the DHW values at the four coral bleaching sites (locations shown on Fig. 9d) throughout time. DHW of all four sites showed continuous increases from 2010 to 2084, with a more centralized distribution of DHW in 2084

Table 7 List of the alert levels at the four coral bleaching sites (Fig. 9) throughout time

Site location	2010	2024	2054	2084
#1	Alert Level 1	Alert Level 2	Alert Level 2	Alert Level 2
#2	Alert Level 1	Alert Level 1	Alert Level 2	Alert Level 2
#3	Alert Level 2	Alert Level 2	Alert Level 2	Alert Level 2
#4	Warning	Warning	Alert Level 1	Alert Level 2

Threshold of each level was based on DHW and associated criteria summarized in Table 5

a waterbody, will remain in the waterbody before exiting (Monsen et al. 2002). Results show that locations corresponding to low water velocities had the largest water retention times, and locations corresponding to both high water retention times and shallow water depths had the greatest increases in SST under future warming scenarios (Fig. 11). These regions typically corresponded to nearshore areas where coral reefs are located. Although water retention times within each 1 km^2 area near regions containing coral reefs typically ranged between 0 and 20 h, the average time these water parcels resided within the bay were typically much greater than this.

Discussion

Model performance on predicting flow and SST

Model validation indicated that the observed ζ and T_w at different locations within the study site were well replicated by the numerical model, with high IAS values. Even though STRI station was the only site where tidal height model performance could be assessed due to the lack of availability of observational data at other locations, accurate tidal predictions at this interior bay site suggested that tidal and flow predictions were reasonably accurate throughout the domain. The predictions on T_w (or equivalently, SST), however, saw noticeable spatial variations in the model agreement with observations, such that COB and CAB had higher IAS values than STRI and ROB. Both COB and CAB were less protected and were more directly influenced by open ocean conditions than the sites located at STRI and ROB. In addition, trends in observed and modeled T_w, as shown in Fig. 6, depict closer agreement at the STRI site than at ROB, likely due to the location of ROB being along the interior of the bay, the furthest distance from the outer boundary where tidal forcing was imposed. However, much fewer coral reefs are located in the vicinity of ROB than other site locations, and therefore, this lower agreement with observations likely had minor impacts on overall heating results under future warming scenarios.

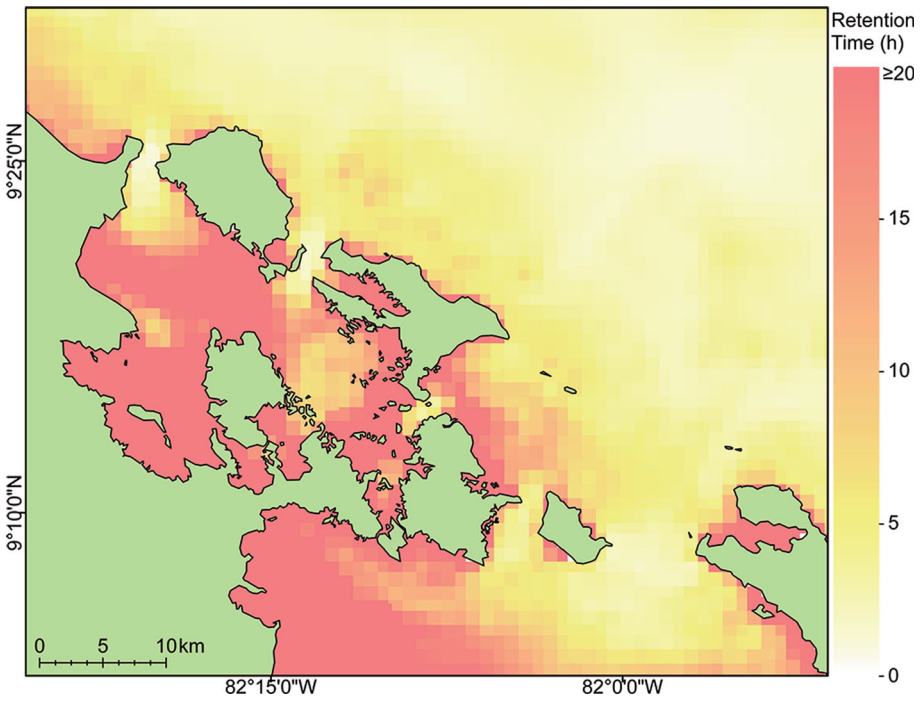

Fig. 11 Average retention time of water masses within equivalent 1 km^2 regions, averaged across a spring-neap cycle for August 2010

Model limitations

Within the numerical model, the accuracy of the predicted flow and SST relies largely upon the quality of the boundary and initial conditions, taken predominately from the STRI station. Although the model did an excellent job in predicting weekly to monthly trends in overall thermal heating and cooling, the model, at times, did a relatively poor job of predicting diurnal temperature variability. It is assumed that data measured at STRI are both accurate and representative of the entire study site. This assumption may poorly reproduce local short-term variability in wind patterns, atmospheric pressure, surface runoff from the land, and precipitation. Furthermore, due to the relatively coarse resolution of bathymetry data applied in the model, the water depth ascribed to near the shorelines, especially those adjacent to many of the small islands, is of lower accuracy. These variables can possibly explain the lower model agreement to measured water temperatures for sites at greater distances from STRI. In addition, the long-term predictions of future global warming scenarios depend largely on the credibility of the IPCC monthly averaged values. As part of the nature of climate predictions, approximations and uncertainties always exist.

The predicted bleaching alert takes into account only the thermal stress under the projected global warming. However, a number of factors influence the susceptibility of corals to bleaching. For example, adaptation by the algal symbionts may increase coral resistance to thermal stress during periods of elevated SST and assist in coral recovery from bleaching afterward (Baker et al. 2004; Little et al. 2004; Rowan 2004). Studies have indicated that some coral reefs may shift to symbiotic algae that are more temperature tolerant as a way to adapt to coral bleaching (Hoegh-Guldberg 2005). Other important factors such as reef morphology, storm events, and sea level rise were also not included in this study.

Thermal stress, coral bleaching, and implications

As predicted by the numerical model, Bocas del Toro Archipelago's SST increased in most locations at about 0.03 °C per year, along with an increase in DHW of more than 0.1 °C weeks on average. The average DHW increase for the four selected bleaching sites was 0.158 °C weeks per year. This result agrees with the predictions of flow patterns that indicate that low water velocity regions within or adjacent to the bay that cause long water retention times are more susceptible to heating under predicted atmospheric warming conditions. Considering that most of the coral reefs were in a bleaching Warning or Alert Level 1 in the 2010 scenario, this trend of increasing SST with time is of substantial environmental concern. Within the modeled 2010 scenario, regions that show Alert Level 1 do not necessarily correlate with locations of highest observed coral bleaching. This may be due to discontinuities in monitoring or reporting of bleaching areas of coral reefs in Bocas del Toro, or may be a result of corals that have adapted to high water temperatures or highly variable water temperatures. For the modeled 2010 scenario, areas of low water velocities and high water retention times tended to have both high SST and high variability in SST, potentially leading to a coral environment of greater thermal resistance (Buddemeier et al. 2004; McClanahan et al. 2007a; Jones et al. 2008).

The spatial distribution of the modeled thermal stress, in addition to its overall temporal trend, demonstrates the importance of geographic variations faced by the corals under predicted climate change scenarios. Even with limited records on specific bleaching events, the bleaching Site 3, recorded in 2002, was no longer recognized as a coral reef site after a 2010 assessment (ReefBase 2013). This follows trends from predicted DHW and bleaching alerts, where an Alert Level 1 was estimated to exist in 2010 where some bleaching is expected, to Alert Level 2 in 2024, which corresponds to the status at which widespread bleaching and coral mortality is expected. DHW estimates, especially those at the four bleaching sites, showed significant spatial variability from 2010 to 2054, ranging from low-level thermal stress to a high mortality threat. By 2084, almost all coral reefs are susceptible to bleaching-induced mortality, except for a region of relatively lower thermal stress along the outer boundary of the archipelago. By 2084, only corals exposed to open ocean currents are predicted to survive, while the inner bays will be completely devoid of coral, if DHW threat warnings prove correct.

The spatial trends in thermal stress within the Panamanian reefs agree with field and numerical studies conducted along a fringing coral reef-lagoon system in Australia where the difference in temperature between the reef and surrounding offshore waters was predominantly a function of both water residence time and the daily mean net heat flux, while diurnal variations in water temperatures were driven by the diurnal fluctuation in the net heat flux (Zhang et al. 2013). Inner lagoon reef temperatures were found to be substantially higher than offshore waters under normal weather conditions, while temperatures across the entire reef were elevated during extreme heating events, which lead to mass coral bleaching. Our findings are also likely applicable to many coral reef regions worldwide, and in particular reefs that are found in shallow and partially enclosed coastal regions with long water retention times.

Based on the susceptibility of these Panamanian coral reefs to bleaching, there is a need to consider the management status of existing marine protected areas (MPA). Current MPAs in this study site were designated within a limited region, located adjacent to Bleaching Site 2 (Fig. 1). While Site 2 was estimated to have Alert Level 1

status until 2024, indicating less severe bleaching, areas close to Site 4 were predicted to be under 'Warning,' and therefore be less susceptible to thermal stress under projected warming scenarios. MPA design criteria often allocate higher priority to areas that are both likely to survive thermal stress due to climate change and have high biodiversity (McClanahan et al. 2007b). Using these predicted scenarios, it is suggested that coral reefs located within regions with shorter water retention times that are exposed to exchange flows with the open ocean, such as Site 4, should be prioritized for MPA management. However, results suggest that we should expect large-scale coral bleaching events, and likely coral die-off, in the coming decades within this Caribbean reef.

Acknowledgments We thank the scientific staff at the Smithsonian Tropical Research Institute in Bocas del Toro, Panama, for providing meteorological and sea surface temperature data. This research was funded by the National Science Foundation (NSF-OCE 1151314) and by the University of Virginia's Deepening Global Education Grant Program.

References

Aronson RB, Precht WF, Toscano MA, Koltes KH (2002) The 1998 bleaching event and its aftermath on a coral reef in Belize. Mar Biol 144:435–447

Ateweberhan M, McClanahan TR (2010) Relationship between historical sea-surface temperature variability and climate change-induced coral mortality in the western Indian Ocean. Mar Pollut Bull 60:964–970

Baird AH, Bhagooli R, Ralph PJ, Takahashi S (2009) Coral bleaching: the role of the host. Trends Ecol Evol 24:16–20

Baker A, Starger CJ, McClanahan T, Glynn PW (2004) Corals' adaptive response to climate change. Nature 430:741

Berkelmans R, Oliver JK (1999) Large-scale bleaching of corals on the Great Barrier Reef. Coral Reefs 18:55–60

Berkelmans R, Weeks SJ, Steinberg CR (2010) Upwelling linked to warm summers and bleaching on the Great Barrier Reef. Limnol Oceanogr 55:2634–2644

Bindoff NL, Willebrand J, Artale V, Cazenave A, Gregory J, Gulev S, Hanawa K, Le Quere C, Levitus S, Nojiri Y, Shum CK, Talley LD, Unnikrishnan A (2007) Observations: Oceanic climate change and sea level. In: Solomon S, Qin D, Manning M, Chen Z, Marquis M, Averyt KB, Tignor M, Miller HL (eds) Climate change 2007: the physical science basis. Contribution of working Group 1 to the Fourth Assessment Report of the Intergovernmental Panel on Climate Change. Cambridge University Press, Cambridge and New York, pp 384–428

Boudreau BP, Jorgensen BB (2001) The Benthic boundary layer: transport processes and biogeochemistry. Oxford University Press, New York

Bradley P, Fisher WS, Bell H (2009) Development and implementation of coral reef biocriteria in U.S. jurisdictions. Environ Monit Assess 150:43–51

Bruno JF, Selig ER, Casey KS, Page CA, Willis BL, Harvell CD, Sweatman H, Melendy AM (2007) Thermal stress and coral cover as drivers of coral disease outbreaks. PLoS Biol 5:e124

Buddemeier RW, Baker AC, Fautin DG, Jacobs JR (2004) The adaptive hypothesis of bleaching. In: Rosenberg E (ed) Coral health and disease. Springer-Verlag, Berlin, pp 427–444

Davis K, Lentz S, Pineda J, Farrar J, Starczak V, Churchill J (2011) Observations of the thermal environment on Red Sea platform reefs: a heat budget analysis. Coral Reefs 30:25–36

Doney SC, Ruckelshaus M, Duffy JE, Barry JP, Chan F, English CA, Galindo HM, Grebmeier JM, Hollowed AB, Knowlton N, Polovina J, Rabalais NN, Sydeman WJ, Talley LD (2012) Climate change impacts on marine ecosystems. Ann Rev Mar Sci 4:1–27

Donner SD (2009) Coping with commitment: projected thermal stress on coral reefs under different future scenarios. PLoS One 4:e5712

Eakin CM, Lough JM, Heron SF (2009) Climate variability and change: monitoring data and evidence for increased coral bleaching stress. In: van Oppen M, Lough JM (eds) Coral bleaching: patterns, processes, causes and consequences. Springer, Heidelberg, pp 41–67

Egbert GD, Erofeeva SY (2002) Efficient inverse modeling of barotropic ocean tides. J Atmos Ocean Tech 19:183–204

Egbert GD, Bennet AF, Foreman MGG (1994) TOPEX/POSEIDON tides estimated using a global inverse model. J Geophys Res 99:24821–24852

ESRI (2010) DeLorme World Base Map 2010. ArcGIS Online. http://www.arcgis.com/home/item.html?id=b165c3df453e4be6b5ac4fdb241effbe

Ferrier-Pages C, Richard C, Forcioli D, Allemand D, Pichon M, Shick JM (2007) Effects of temperature and UV radiation increases on the photosynthetic efficiency in four scleractinian coral species. Biol Bull 213:76–87

Garratt JR (1977) Review of drag coefficients over oceans and continents. Mon Weather Rev 105:915–929

Gill AE (1982) Atmosphere-Ocean dynamics. Academic Press 662 pp

Glynn PW (1993) Coral-reef bleaching - ecological perspectives. Coral Reefs 12:1–17

Green EP, Short FT (2003) World atlas of seagrasses. Prepared by the UNEP-WCMC. University of California Press, Berkley, USA

Grena R (2012) Five new algorithms for the computation of sun position from 2010 to 2110. Sol Energy 86:1323–1337

Guzmán H, Barnes PAG, Lovelock CE, Feller IC (2005) A site description of the CARICOMP mangrove, seagrass and coral reef sites in Bocas del Toro, Panama. Caribb J Sci 44:430–440

Hannah DM, Malcolm IA, Soulsby C, Youngson AF (2004) Heat exchanges and temperatures within a salmon spawning stream in the Cairngorms, Scotland: seasonal and sub-seasonal dynamics. River Res Appl 20:635–652

Hannah DM, Malcolm IA, Soulsby C, Youngson AF (2008) A comparison of forest and moorland stream microclimate, heat exchanges and thermal dynamics. Hydrol Process 22:919–940

Harvell CD, Mitchell CE, Ward JR, Altizer S, Dobson AP, Ostfeld RS (2002) Climate warming and disease risks for terrestrial and marine biota. Science 296:2158–2162

Heaps NS (1965) Storm surges on a continental shelf. Philos Trans A Math Phys Eng Sci 257:351–383

Hoegh-Guldberg O (1999) Climate change, coral bleaching and the future of the world's coral reefs. Mar Freshw Res 50:839–866

Hoegh-Guldberg O (2005) Low coral cover in a high-CO2 world. J Geophys Res C 110:C09S06

Hoegh-Guldberg O (2011) The impact of climate change on coral reef ecosystems. In: Dubinsky Z, Stambler N (eds) Coral reefs: an ecosystem in transition. Springer, Dordrecht, Netherlands, pp 391–403

Hoegh-Guldberg O, Mumby PJ, Hooten AJ, Steneck RS, Greenfield P, Gomez E, Harvell CD, Sale PF, Edwards AJ, Caldeira K, Knowlton N, Eakin CM, Iglesias-Prieto R, Muthiga N, Bradbury RH, Dubi A, Hatziolos ME (2007) Coral reefs under rapid climate change and ocean acidification. Science 318:1737–1742

Hughes TP, Baird AH, Bellwood DR, Card M, Connolly SR, Folke C, Grosberg R, Hoegh-Guldberg O, Jackson JBC, Kleypas J, Lough JM, Marshall P, Nystrom M, Palumbi SR, Pandolfi JM, Rosen B,

Roughgarden J (2003) Climate change, human impacts, and the resilience of coral reefs. Science 301:929–933
IMaRS-USF (2005) Millennium Coral Reef Mapping Project. UNEP World Conservation Monitoring Centre. Cambridge, UK. http://data.unep-wcmc.org/datasets/13
IMaRS-USF and IRD (2005) Millennium Coral Reef Mapping Project. UNEP World Conservation Monitoring Centre. Cambridge, UK. http://data.unep-wcmc.org/datasets/13
IPCC (2003) Future climate in world regions: an intercomparison of model-based projections for the new IPCC emissions scenarios. The Intergovernmental Panel on Climate Change. http://www.ipcc-data.org/ddc_visualisation.html
IUCN and UNEP-WCMC (2010) The World Database on Protected Areas (WDPA). UNEP-WCMC, Cambridge, UK. http://www.protectedplanet.net
Jokiel PL, Brown EK (2004) Global warming, regional trends and inshore environmental conditions influence coral bleaching in Hawaii. Glob Chang Biol 10:1627–1641
Jones AM, Berkelmans R, van Oppen MJH, Mieog JC, Sinclair W (2008) A community change in the algal endosymbionts of a scleractinian coral following a natural bleaching event: field evidence of acclimatization. Proc R Soc Lond B Biol Sci 275:1359–1365
Kauffman KW, Thomson RC (2005) Water temperature variation and the meteorological and hydrographic environment of Bocas del Toro, Panama. Caribb J Sci 41:392–413
Kernkamp HWJ, Petit HAH, Gerritsen H, de Goede ED (2005) A unified formulation for the three-dimensional shallow water equations using orthogonal co-ordinates: theory and applications. Ocean Dynamics 55:351–369
Lesser MP (1996) Exposure of symbiotic dinoflagellates to elevated temperatures and ultraviolet radiation causes oxidative stress and inhibits photosynthesis. Limnol Oceanogr 41:271–283
Lesser MP, Farrell JH (2004) Exposure to solar radiation increases damage to both host tissues and algal symbionts of corals during thermal stress. Coral Reefs 23:367–377
Lesser MP, Stochaj WR, Tapley DW, Shick JM (1990) Bleaching in coral reef anthozoans: effects of irradiance, ultraviolet radiation, and temperature on the activities of protective enzymes against active oxygen. Coral Reefs 8:225–232
Lesser GR, Roelvink JA, van Kester J, Stelling GS (2004) Development and validation of a three-dimensional morphological model. Coast Eng 51:883–915
Levitus S, Antonov JI, Boyer TP, Locarnini RA, Garcia HE, Mishonov AV (2009) Global ocean heat content 1955–2008 in light of recently revealed instrumentation problems. Geophys Res Lett 36:L07608
Little AF, van Oppen MJ, Willis BL (2004) Flexibility in algal endosymbioses shapes growth in reef corals. Science 304:1492–1494
Liu G, Strong AE, Skirving W, Arzayus LF (2006) Overview of NOAA coral reef watch program's near-real time satellite global coral bleaching monitoring activities. Proc 10th Int Coral Reef Symp 1:1783–1793
Madsen J, Chambers P, James W, Koch E, Westlake D (2001) The interaction between water movement, sediment dynamics and submersed macrophytes. Hydrobiologia 444:71–84
Manzello DP, Brandt M, Smith TB, Lirman D, Hendee JC, Nemeth RS (2007) Hurricanes benefit bleached corals. Proc Natl Acad Sci USA 104:12035–12039
McClanahan TR, Graham NAJ, Calnan JM, MacNeil MA (2007a) Toward pristine biomass: reef fish recovery in coral reef marine protected areas in Kenya. Ecol Appl 17:1055–1067
McClanahan TR, Ateweberhan M, Muhando CA, Maina J, Mohammed MS (2007b) Effects of climate and seawater temperature variation on coral bleaching and mortality. Ecol Monogr 77:503–525
Monsen NE, Cloern JE, Lucas LV, Monismith SG (2002) A comment on the use of flushing time, residence time, and age as transport time scales. Limnol Oceanogr 47:1545–1553
Muller EM, Rogers CS, Spitzack AS, van Woesik R (2008) Bleaching increase likelihood of disease on Acropora palmata (Lamarck) in Hawksnest Bay, St. John, US Virgin Islands. Coral Reefs 27:191–195
Peñaflor EL, Skirving WJ, Strong AE, Heron SF, David LT (2009) Sea-surface temperature and thermal stress in the Coral Triangle over the past two decades. Coral Reefs 28:841–850
Prager EJ (1991) Numerical simulation of circulation in a Caribbean-type backreef lagoon. Coral Reefs 10:177–182
Pratchett MS, Wilson SK, Graham NAJ, Munday PL, Jones GP, Polunin NVC (2009) Coral bleaching and consequences for motile reef organisms: Past, present and uncertain future effects. In: van Oppen M, Lough J (eds) Coral bleaching: patterns and processes, causes and consequences. Springer, Heidelberg, pp 139–158
Reaser JK, Pomerance R, Thomas PO (2000) Coral bleaching and global climate change: scientific findings and policy recommendations. Conserv Biol 14:1500–1511
ReefBase (2013) A Global Information System for Coral Reefs. http://www.reefbase.org
Rehr AP (2012) A decision support framework for science-based, multi-stakeholder deliberation: a coral reef example. Environ Manage 50:1204–1218
Reidenbach MA, Monismith SG, Koseff JR, Yahel G, Genin A (2006) Boundary layer turbulence and flow structure over a fringing coral reef. Limnol Oceanogr 51:1956–1968
Reynolds RW, Smith TM (1994) Improved global sea surface temperature analysis using optimal interpolation. J Clim 7:929–948
Reynolds RW, Zhang HM, Smith TM, Gentemann CL, Wentz F (2005) Impact of in situ and additional satellite data on the accuracy of a sea-surface temperature analysis for climate. Int J Climatol 25:857–864
Rowan R (2004) Coral bleaching: Thermal adaptation in reef coral symbionts. Nature 430:742
Stelling GS (1984) On the construction of computational methods for shallow water flow problems. Rijkswaterstaat Commun 35, The Hague, Netherlands
Strong AE, Arzayus F, Skirving W, Heron SF (2006) Identifying coral bleaching remotely via Coral Reef Watch–improved integration and implications for changing climate. In: Phinney JT, Hoegh-Guldberg O, Kleypas J, Skirving W, Strong A (eds) Coral reefs and climate change: science and management, coastal and estuarine studies 61. American Geophysical Union, Washington, D.C, pp 163–180
Thur SM (2010) User fees as sustainable financing mechanisms for marine protected areas: an application to the Bonaire National Marine Park. Mar Policy 34:63–69
UNEP-WCMC, Short FT (2005) Global distribution of seagrasses. V2.0. http://www.arcgis.com/home/item.html?id=de158acb9f884db3bff1a39dd056913b
UNEP-WCMC, WorldFish Centre, World Resources Institute, The Nature Conservancy (2010) Global distribution of warmwater coral reefs, compiled from multiple sources, including the Millennium Coral Reef Mapping Project. UNEP World Conservation Monitoring Centre. Cambridge, UK. http://data.unep-wcmc.org/datasets/13
Walther GR, Post E, Convey P, Menzel A, Parmesan C, Beebee TJC, Fromentin JM, Hoegh-Guldberg O, Bairlein F (2002) Ecological responses to recent climate change. Nature 416:389–395
Warner JC, Sherwood CR, Arango HG, Signell RP (2005) Performance of four turbulence closure models implemented using a generic length scale method. Ocean Modeling 8:81–113

Webb BW, Zhang Y (1999) Water temperatures and heat budgets in Dorset chalk water courses. Hydrol Process 13:309–321

Wells JR, Fram JP, Pawlak G (2012) Solar warming of near-bottom water over a fringing reef. J Mar Res 70:641–660

Wilkinson CR (1996) Global change and coral reefs: Impacts on reefs, economies and human cultures. Glob Chang Biol 2:547–558

Willmott CJ (1982) Some comments on the evaluation of model performance. Bull Am Meteorol Soc 63:1309–1369

Zhang Z, Falter J, Lowe R, Ivey G, McCulloch M (2013) Atmospheric forcing intensifies the effects of regional ocean warming on reef-scale temperature anomalies during a coral bleaching event. J Geophys Res 118:4600–4616